Biosensing

DOI: 10.1002/ange.201400900

Real-Time In Vivo Quantitative Monitoring of Drug Release by Dual-Mode Magnetic Resonance and Upconverted Luminescence Imaging**

Jianan Liu, Jiwen Bu, Wenbo Bu, Shengjian Zhang, Limin Pan, Wenpei Fan, Feng Chen, Liangpin Zhou, Weijun Peng, Kuaile Zhao, Jiulin Du, and Jianlin Shi**

Abstract: *Insufficient or excess drug doses, due to unknown actual drug concentrations at the focus, are one of the main causes of chemotherapy failure for cancers. In this regard, the real-time monitoring of the release of anticancer drugs from nanoparticle drug delivery systems is of crucial importance, but it remains a critical and unsolved challenge. Herein, we report the proposal and development of a novel concept of real-time monitoring of NIR-triggered drug release in vitro and in vivo by using simultaneous upconverted luminescence (UCL) and magnetic resonance (MR) imaging. Such a monitoring strategy features the high sensitivity of UCL and the high-resolution, noninvasiveness, and tissue-depth-independence of MR imaging. The dual-mode real-time and quantitative monitoring of drug release can be applied to determine online the drug concentrations in vivo in the tissue regions of interest and, therefore, to avoid insufficient or excess drug dosings.*

The unknown actual drug concentrations at in vivo focuses have puzzled doctors since the invention of chemodrugs. In fact, it is highly preferred in clinics that the drug release profile can be monitored in a quantitative manner in real time to avoid insufficient or excess drug dosings at the focuses; real-time quantitative monitoring is a great aid in the decision making of doctors for patient-specific drug administration and benefits the effectiveness and success of cancer therapy. The best way to monitor drug release is to follow the drug molecules themselves. Among all of the current diagnostic tools, positron emission tomography (PET) is one of the few applicable protocols for following drugs containing a radionuclide (for example, ^{18}F, ^{11}C, and ^{15}O) within their structure.[1] Unfortunately, at the moment few drugs can meet such a harsh precondition. Another possible way to track drug release is to develop an optical imaging strategy, which is, so far, the most sensitive technique. For example, a number of drug delivery systems (DDSs) have been developed for fluorescence monitoring of anticancer drug release by a photocaged compound[2] or fluorescence resonance energy transfer (FRET) monitoring between the donor (that is, the DDS) and the acceptor (that is, the drug).[3] However, this technique uses UV or visible light as the excitation source and is severely limited for in vivo applications because of the very low penetration depth in living tissues due to strong light absorption and scattering. Therefore, it would be preferred to use NIR light as the excitation source to monitor the release of anticancer drugs.

Upconversion nanoparticles (UCNPs) have emerged as appealing candidates for donors that use a NIR continuous-wave (CW) diode laser as an excitation source, which can achieve increased penetration depth and suppress autofluorescence in biological samples.[4] By emitting UV or visible light, which is needed for certain photoreactions, UCNPs have been used as nanotransducers for photodynamic therapy (PDT)[5] and to detect trace amounts of avidin[6] and the release of caged compounds.[7] Therefore, a NIR-excitation technology based on UCNPs may offer a potential way to monitor drug release by luminescence resonance energy transfer (LRET) between the donor UCNPs and the acceptor fluorescent drugs. Although such optical strategies are rather sensitive, they are limited to using light-absorbing drugs like doxorubicin (DOX) as model cargoes; unfortunately, most of the current drug candidates are not light absorbent. As a result, classical single-mode fluorescence sensors are, in most cases, not applicable for the real-time monitoring of drug release.

Of the various currently available imaging modalities, magnetic resonance imaging (MRI), as a powerful technique for tomographic imaging of biological targets, appears to be an excellent tool for monitoring drug delivery because it can produce noninvasive, tissue-depth-independent images with high spatial and temporal resolutions that are sufficient for measuring changes in the distribution of drugs despite the relatively low sensitivity. Given the above considerations, it would be highly desirable to develop simpler, more sensitive,

[*] Dr. J. N. Liu, Prof. W. B. Bu, Dr. L. M. Pan, Dr. W. P. Fan, Dr. F. Chen, Prof. J. L. Shi
State Key Laboratory of High Performance Ceramics and Superfine Microstructure
Shanghai Institute of Ceramics, Chinese Academy of Sciences
1295 Ding-xi Road, Shanghai 200050 (China)
E-mail: wbbu@mail.sic.ac.cn
jlshi@mail.sic.ac.cn
Dr. J. W. Bu, Prof. J. L. Du
Institute of Neuroscience and State Key Laboratory of Neuroscience
Shanghai Institutes for Biological Sciences
Chinese Academy of Sciences
320 Yue-Yang Road, Shanghai 200031 (China)
Dr. S. J. Zhang, Prof. L. P. Zhou, Prof. W. J. Peng, Prof. K. L. Zhao
Department of Radiology
Fudan University Cancer Hospital, Fudan University
Shanghai 200032 (China)

[**] This work has been financially supported by the National Natural Science Foundation of China (grant nos. 51372260, 51132009, 21172043, 51072212, and 51102259), the Shanghai Rising-Star Program (grant no. 12QH1402500), the Nano special program of the Science and Technology Commission of Shanghai (grant no. 11nm0505000), and the Development Foundation for Talents of Shanghai (grant no. 2012035).

Supporting information for this article is available on the WWW under http://dx.doi.org/10.1002/anie.201400900.

and noninvasive sensors for the real-time monitoring of drug delivery by MRI techniques, which would simultaneously enable MRI-guided surgical therapy of diseases and even the evaluation of therapy outcome in living cells/tissues. However, there is no report about monitoring drug release by using MRI techniques in real time.

Herein, we report the synthesis of multifunctional $NaYF_4$:Yb/Tm@$NaGdF_4$ core/hollow mesoporous silica shell nanoparticles (designated as UCNP@hmSiO_2) and their application in simultaneous NIR-triggered drug delivery and in situ quantitative drug release monitoring by both upconverted luminescence (UCL) and longitudinal relaxation time (T_1) MR imaging in real time. Scheme 1 illustrates the

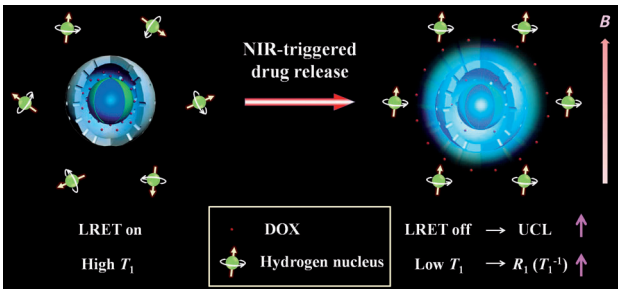

Scheme 1. With anticancer drugs (DOX) fully loaded into the mesopores and hollow cavity, UCL signals are quenched through LRET between UCNPs and DOX under 980 nm excitation; the T_1-MR signals are almost undetectable due to the low probability of water molecules bonding to the Gd^{3+} ions. Upon NIR-triggered drug release from the nanosensors, both the UCL and T_1-MR signals will be restored accordingly. As a result, drug release can be detected by the designed UCL/T_1-MRI dual-mode nanosensor.

prototype nanosensors developed for monitoring NIR-triggered drug delivery, which contain three essential components: 1) modified azobenzene (azo) on the mesopore surface of UCNP@hmSiO_2 to contribute to NIR-triggered drug release;[8] 2) the LRET donor–acceptor pair of the UCNP and DOX, designed for monitoring NIR-controlled drug release in real time by detecting UCL signals; 3) the presence of the anticancer drug residing in the hollow cavity to allow the T_1-MR effect for monitoring NIR-controlled drug release in real time by detecting MR signals. It is worth noting that our previous work focused on the effectiveness of NIR-triggered drug release control,[8] whereas, in the present study, we redesigned a nanosensor based on hollow-structured nanocomposites and, more importantly, the models for real-time monitoring of drug release in vitro and in vivo by both MR and UCL imaging have been established by using such a nanosensor.

The overall synthesis of UCNP@hmSiO_2 is shown in Figure 1 a. Oleic acid stabilized UCNPs were synthesized by a thermal decomposition method.[9] Subsequently, the UCNPs were incorporated into reverse micelles containing cyclohexane and Igepal CO-520. Addition of tetraethylorthosilicate (TEOS) to the mixture initiated the controlled sol–gel reaction at room temperature, which led to the formation of dense silica shells (designated as UCNP@dSiO_2).[10] A mesoporous silica shell was deposited onto the surface of the

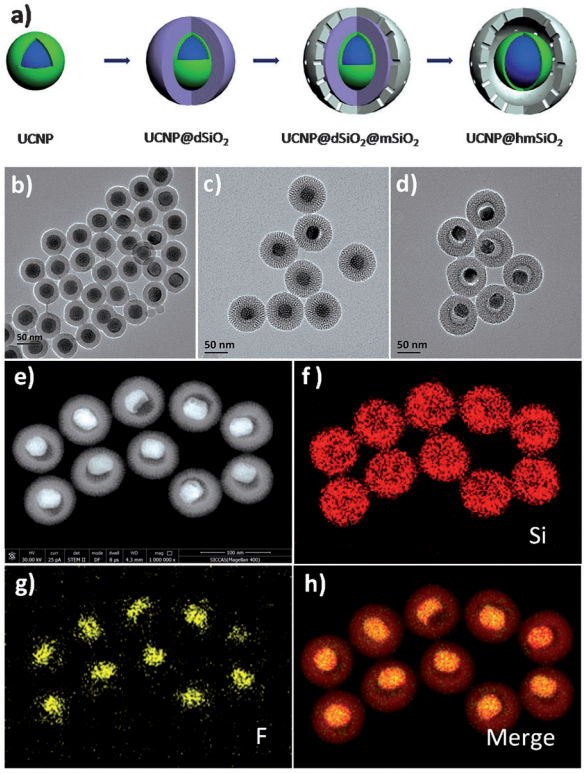

Figure 1. a) The formation process of UCNP@hmSiO_2. b–d) TEM images of b) UCNP@dSiO_2, c) UCNP@dSiO_2@mSiO_2, and d) UCNP@hmSiO_2. e–h) STEM images and corresponding elemental (F, Si) mappings of UCNP@hmSiO_2.

UCNP@dSiO_2 through hydrolysis of TEOS and self-assembly with the cetyltrimethylammonium chloride (CTAC) template,[11] to form UCNP@dSiO_2@mSiO_2. Finally, template-extracted UCNP@dSiO_2@mSiO_2 was directly tuned to hollow mesoporous silica by incubation in water at 95 °C for 2 h through a "surface-protected etching" process.[12] To date, it still remains a great challenge to synthesize hmSiO_2-based nanoparticles smaller than 100 nm because small-sized nanoparticles are more fragile to alkaline etchants (such as $NaCO_3$) than their larger counterparts (> 150 nm). Based on the "structural-difference-based selective etching" methods previously developed by our group[13] and other researchers,[14] hot water was chosen as a mild etchant[15] to selectively remove the dense silica layer by breaking the Si–O–Si bonds at a controllable rate, with the poly(vinylpyrrolidone)-protected porous silica shell being unaffected.

To enhance the UCL signal and T_1-MR contrast, a thin $NaGdF_4$ shell was coated on the $NaYF_4$:Yb/Tm core nanoparticles,[16] to obtain $NaYF_4$:Yb/Tm@$NaGdF_4$ core–shell nanoparticles (Figure S1 in the Supporting Information). Figure 1 b–d and Figure S2–S4 present TEM and SEM images of all of the products, which exhibit the monosize and monodispersity features of the nanoparticles, and the scanning transmission electron microscopy (STEM) image in Figure 1 e clearly demonstrates the hollow structure between the UCNP cores and the mesoporous silica shells in UCNP@hmSiO_2. Furthermore, elemental mappings by STEM measurements confirm that the UCNPs are located

within the core of the $hmSiO_2$ shells (Figure 1 f–h). The existence of the hollow structure was further confirmed by nitrogen adsorption–desorption analysis (Figure S5 and Table S1), which indicated that the pore volume, BET surface area, and pore-size distribution of UCNP@$hmSiO_2$ are 1.14 $cm^3 g^{-1}$, 556.8 $m^2 g^{-1}$, and 4.4 nm, respectively. The actual Gd content in UCNP@$hmSiO_2$ was calculated to be 1.7 wt% by inductively coupled plasma optical emission spectrometry (ICP-OES). As determined by dynamic light scattering (Figure S6), the UCNP@$hmSiO_2$ particles are approximately 100 nm in diameter with no observable aggregations. The emission spectrum of UCNP@$hmSiO_2$ (Figure S7) displays the characteristic UV and blue emission bands that correspond to the transition from the emitting energy levels of Tm ions. The longitudinal relaxivity (r_1) of UCNP@$hmSiO_2$ was calculated to be 12.29 $mM^{-1} s^{-1}$. This relaxivity is significantly higher than that measured for UCNP@$dSiO_2$@$mSiO_2$ (3.58 $mM^{-1} s^{-1}$; Figure S8 and Table S2 and S3), mainly due to the absence of the dense silica layer in between the Gd-UCNP core and the mesoporous silica shell in UCNP@$hmSiO_2$, which facilitates water molecules bonding to the Gd^{3+} ions.

To control the drug release by NIR light, the mesopores of UCNP@$hmSiO_2$ were covalently linked with "photomechanical" azo groups that act as "stirrers", to form UCNP@$hmSiO_2$-azo,[8] as confirmed by FTIR results (Figure S10). To investigate the NIR-induced drug release behavior from UCNP@$hmSiO_2$, the fluorescent drug DOX and nonfluorescent drug cisplatin (CDDP) were employed as cargoes, respectively. Due to the hollow cavity existing between UCNP and the outer mesoporous silica shell, the anticancer drugs DOX and CDDP could be loaded into UCNP@$hmSiO_2$-azo with high loading efficiencies, which reach 7 and 6 wt%, respectively. The resultant nanoparticles were designated as nanosensor 1 and nanosensor 2, respectively. Under NIR exposure, a significant release of anticancer drugs (DOX or CDDP) can be found, which suggests that the diffusion of anticancer drugs was NIR irradiation dependent (Figure S11).

Based on the well-matched wavelength (Figure 2a) between the upconverted emission of the UCNPs (450 nm/477 nm) and absorption of DOX (480 nm), we explored the potential of the nanosensors for monitoring drug release by measuring the UCL signals in real time. As shown in Figure 2b and Figure S12, the UCNP emission at 450 and 477 nm is completely quenched by both the strong absorption of DOX loaded in the nanosensors and the weak absorption of azo in mesopores. Compared with UCNP@$hmSiO_2$, DOX-UCNP@$hmSiO_2$ emits relatively weak visible light, whereas the UV emission remains unaffected, as confirmed by Figure S13. Hence, although DOX will absorb large amount of upconverted visible light, the unaffected UV light and the remaining visible light will still be effective to trigger the photoisomerization effect of azo. It is known that LRET will not significantly occur if the distance between donors and acceptors is larger than 10 nm. DOX release from the mesopores and hollow cavity resulted in an increased distance of beyond 10 nm between DOX and the UCNP core, which substantially weakens the LRET effect. As a result, the upconversion emission intensities at 450 and 477 nm will gradually recover upon drug release. These results indicate that the UCL signals are sufficiently sensitive to be used as imaging probes for detecting the controlled drug release. Figure 2c summarizes the results of the validation study. The UCL signal intensity (y) at blue wavelengths (intensity arithmetic addition at 450 nm and 477 nm) shows an excellent linear relationship with the amount of released drug (x): $y = 7.69 \times -24.3$. The above results reveal that the UCL signal of nanosensor 1 is a high-performance reporter that, through LRET, can be used to quantitatively measure the amount of released drug.

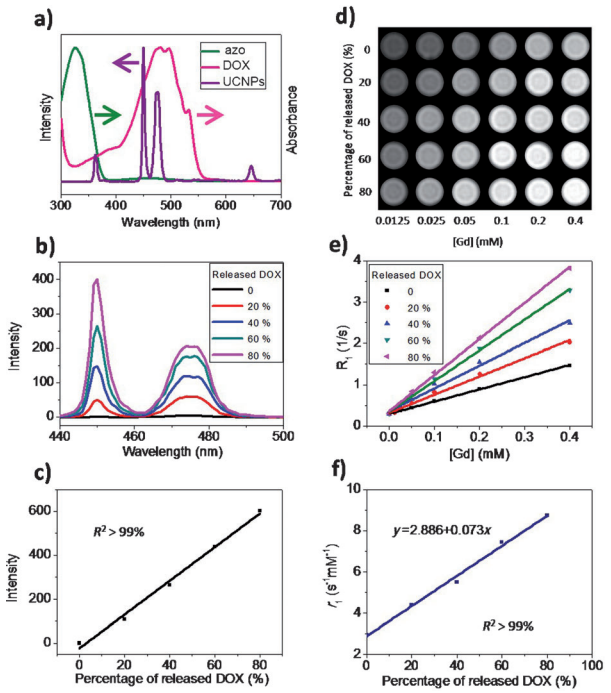

Figure 2. a) Upconversion emission spectrum of UCNPs and the UV/Vis absorption spectrum of DOX and azo. b) Changes in blue (450 and 477 nm) fluorescence of nanosensor 1 upon NIR exposure for different time durations. c) Linear correlation between the percentage of DOX released and the change in the additive UCL intensity of the signals at 450 and 477 nm. d) T_1-MRI results obtained from aqueous suspensions of nanosensor 1 before and after NIR exposure for different time durations. e) Plot of T_1^{-1} versus Gd concentration for nanosensor 1 before and after NIR exposure for different time durations. The calculated r_1 values from black to pink are 2.96, 4.40, 5.50, 7.43, and 8.75 $mM^{-1} s^{-1}$, respectively. f) Linear correlation between the released percentage of DOX and the corresponding r_1 value of nanosensor 1.

To evaluate whether the MR signals can report on the amount of released drug, nanosensor 1 was imaged before and after the release of DOX by using a clinical MRI scanner at 3 T. First, we tested the sensitivity of the nanosensors for probing drug release in phosphate-buffered saline (PBS; Figure 2d). We observed a significant drop in the r_1 value, from 12.29 (Figure S8) to 2.96 $mM^{-1} s^{-1}$ (Figure 2e), after DOX was loaded into the hollow cavity and mesopores due to the decreased probability of water molecules bonding to the Gd^{3+} ions. As expected, a corresponding increase in the T_1-MR signal intensity can be observed upon release of DOX.

The release of various amounts of DOX (20, 40, 60, or 80 wt%) led to gradual recovery of the DOX-quenched T_1-MRI signal corresponding to increments of the r_1 value of 48, 86, 151, and 196%, respectively. This can be clearly attributed to the fact that the DOX release gradually leaves more room in the hollow cavity and mesopores, which favors the diffusion and access of water molecules from outside to the Gd-UCNP core and, consequently, the gradually enhanced relaxation effect of water molecules in the vicinity of the nanoparticles. The excellent linear relationship between the percentage of released DOX and the r_1 value (Figure 2 f) strongly suggests that nanosensor 1 is capable of monitoring the drug release in real time. We next tested the drug-release-dependent T_1-MR behavior of nanosensor 2. As shown in Table S4–S8 and Figure S14 and S15, all of the results demonstrate that T_1-MR signal intensity is enhanced upon CDDP release, which is in excellent agreement with the results observed with DOX. Our studies imply that this carefully designed nanosensor is applicable to monitoring the release behavior of various drugs.

To determine whether nanosensors can produce the UCL and T_1-MR signals of drug release in vitro, HeLa cells were incubated with nanosensor 1 and then exposed to NIR irradiation. As expected, a time-course fluorescence intensity enhancement of DOX in the cancer cells clearly indicates the controlled release of drugs from nanosensor 1 and, in the meantime, the DOX-release-induced UCL signal recovery is clearly detectable (Figure 3 a and Movie S1 (DOX signal) and Movie S2 (UCL signal)). The above observations are more visibly confirmed by the line scanning profiles of fluorescence intensity for selected HeLa cells (Figure 3 b and c). We next examined the suitability of nanosensor 1 as a T_1-MRI nanosensor for monitoring anticancer drug release in cells. As shown in Figure 3 d, the T_1-MR signals of the NIR-exposed cells are apparently stronger than those of the unexposed cells because of the increased probability of water molecules bonding to Gd^{3+} ions due to the NIR-triggered drug release. In addition, similar results were observed in HeLa cells incubated with nanosensor 2 under NIR exposure for various time durations (Figure S20), which further confirmed the applicability of such nanosensors in monitoring the release of different types of drug molecule.

We choose zebrafish as an in vivo model for optical monitoring due to the benefits associated with convenient optical imaging of the model.[17] Zebrafish embryos injected with nanosensor 1 into their heart ventricles showed no apparent DOX and UCL signals in the vascular system of the zebrafish (Figure 4 a), which indicated that the anticancer drug DOX cannot be released without NIR exposure. Interestingly, nanosensor 1 showed significantly brightened UCL signals (Figure 4 a and Movie S3) in the zebrafish heart regions when exposed to NIR light for 60 min; these signals resulted from the NIR-triggered drug release, as confirmed by the clearly intensified DOX signal in the zebrafish vessels (Figure 4 a and Movie S4). Correspondingly, NIR-excited zebrafish demonstrate an approximately 51% enhancement in the T_1-MR signal intensity over those of the control (Figure S24), which is consistent with the in vitro results. To demonstrate the effectiveness of the nanosensors in monitoring drug release with high tissue penetration in vivo by using MRI, we subcutaneously injected nanosensor 2 into walker-256 tumor-bearing rats and recorded the change of T_1-MR signal intensity along with the NIR-triggered drug release. The T_1-MRI results of the rats in the drug release group demonstrate clear enhancements in the T_1-MR signal intensity under NIR exposure (Figure 4 b) relative to those of the control and non-NIR-excited groups (Figure S25). Furthermore, a linear relationship between the MR signal intensity and the corresponding amount of released drugs can be obtained (Figure S26).

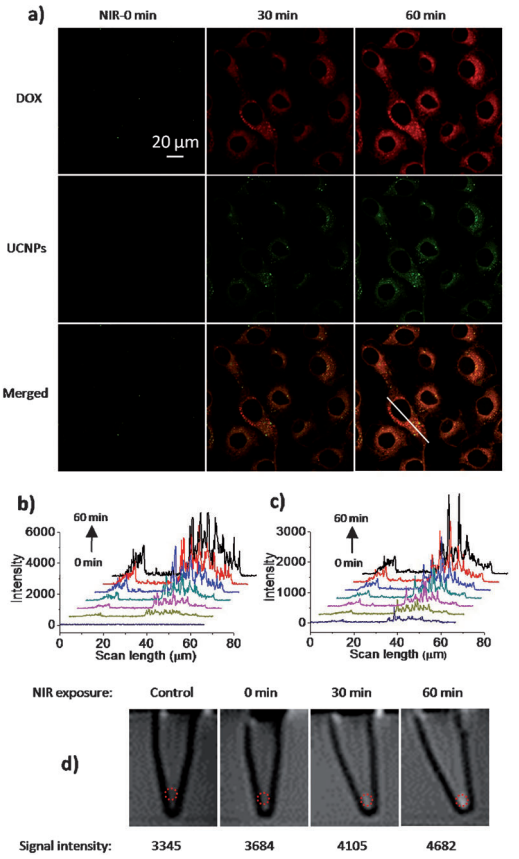

Figure 3. a) Confocal microscopic images showing the change in DOX and UCL signal intensities in HeLa cells. DOX and UCL signals were collected at 500–600 nm and 400–500 nm under excitation of 488 nm and 980 nm lasers, respectively. All images share the same scale bar (20 μm). b and c) Line-scanning profiles of b) DOX and c) UCNP fluorescence intensities on selected HeLa cells in (a). d) MR images shows the intensity change in the R_1 signal in HeLa cells incubated with nanosensor 1 after NIR exposure for different time durations. The power density of the NIR light, which triggered DOX release, is 1.5 $W cm^{-2}$.

In the study described above, we demonstrate that UCNPs ($NaYF_4$:Yb/Tm@$NaGdF_4$) embedded in the core of hollow mesoporous silica nanoparticles can be used as robust nanosensors to visualize and quantify drug release in vitro and in vivo by simultaneous UCL and T_1-MR imaging in real time. Unlike conventional optical imaging of drug delivery, this LRET-based sensor exhibits no autofluorescence and photobleaching from biological samples. Attractively, one great advantage of this nanosensor is that the drug releases can be

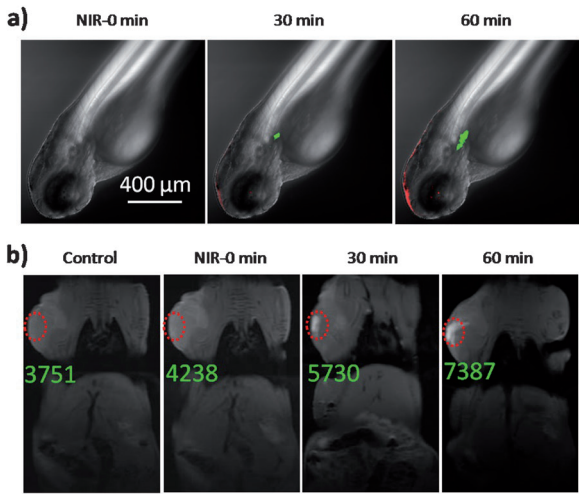

Figure 4. a) Confocal laser scanning microscopy images of zebrafish, in which UCNP signals are green and DOX signals are red. All of the images share the same scale bar (400 μm). b) T_1-MR images of a walker-256 tumor-bearing Sprague Dawley rat injected with nanosensor 2 (1 mg mL^{-1}, 100 μL) subcutaneously before and after NIR exposure for different time durations ($n=3$). The red circles indicate the tumor area where nanosensor 2 were injected. The T_1-MR signal intensities before and after NIR exposure are also provided in the figures. The power density of NIR light employed was 1.5 W cm^{-2}.

quantitatively monitored both in vitro and in vivo by using a 3 T MR scanner, which can be readily translated from mice to humans. The corelationships between the drug release amounts and the MR/UCL signal intensities are independent of the type of DDSs, so we anticipate that such monitoring strategies can be applied to other DDSs with drug release being controlled or not controlled.

Received: January 27, 2014
Published online: March 25, 2014

Keywords: drug delivery · imaging · LRET · nanoparticles · sensing

[1] F. Brady, S. K. Luthra, G. D. Brown, S. Osman, E. Aboagye, A. Saleem, P. M. Price, *Curr. Pharm. Des.* **2001**, *7*, 1863.
[2] A. Jana, K. S. P. Devi, T. K. Maiti, N. D. P. Singh, *J. Am. Chem. Soc.* **2012**, *134*, 7656.
[3] a) R. Weinstain, E. Segal, R. Satchi-Fainaro, D. Shabat, *Chem. Commun.* **2010**, *46*, 553; b) J. Lai, B. P. Shah, E. Garfunkel, K.-B. Lee, *ACS Nano* **2013**, *7*, 2741.
[4] a) M. Haase, H. Schäfer, *Angew. Chem.* **2011**, *123*, 5928; *Angew. Chem. Int. Ed.* **2011**, *50*, 5808; b) F. Wang, R. Deng, J. Wang, Q. Wang, Y. Han, H. Zhu, X. Chen, X. Liu, *Nat. Mater.* **2011**, *10*, 968; c) F. Wang, Y. Han, C. S. Lim, Y. H. Lu, J. Wang, J. Xu, H. Y. Chen, C. Zhang, M. H. Hong, X. G. Liu, *Nature* **2010**, *463*, 1061.
[5] a) N. M. Idris, M. K. Gnanasammandhan, J. Zhang, P. C. Ho, R. Mahendran, Y. Zhang, *Nat. Med.* **2012**, *18*, 1580; b) Y. I. Park, H. M. Kim, J. H. Kim, K. C. Moon, B. Yoo, K. T. Lee, N. Lee, Y. Choi, W. Park, D. Ling, K. Na, W. K. Moon, S. H. Choi, H. S. Park, S.-Y. Yoon, Y. D. Suh, S. H. Lee, T. Hyeon, *Adv. Mater.* **2012**, *24*, 5755.
[6] D. Tu, L. Liu, Q. Ju, Y. Liu, H. Zhu, R. Li, X. Chen, *Angew. Chem.* **2011**, *123*, 6430; *Angew. Chem. Int. Ed.* **2011**, *50*, 6306.
[7] a) C. J. Carling, F. Nourmohammadian, J. C. Boyer, N. R. Branda, *Angew. Chem.* **2010**, *122*, 3870; *Angew. Chem. Int. Ed.* **2010**, *49*, 3782; b) M. K. G. Jayakumar, N. M. Idris, Y. Zhang, *Proc. Natl. Acad. Sci. USA* **2012**, *109*, 8483; c) J. V. Garcia, J. Yang, D. Shen, C. Yao, X. Li, R. Wang, G. D. Stucky, D. Zhao, P. C. Ford, F. Zhang, *Small* **2012**, *8*, 3800.
[8] J. Liu, W. Bu, L. Pan, J. Shi, *Angew. Chem.* **2013**, *125*, 4471; *Angew. Chem. Int. Ed.* **2013**, *52*, 4375.
[9] F. Chen, W. Bu, S. Zhang, J. Liu, W. Fan, L. Zhou, W. Peng, J. Shi, *Adv. Funct. Mater.* **2013**, *23*, 298.
[10] F. Chen, W. Bu, S. Zhang, X. Liu, J. Liu, H. Xing, Q. Xiao, L. Zhou, W. Peng, L. Wang, J. Shi, *Adv. Funct. Mater.* **2011**, *21*, 4285.
[11] L. Pan, Q. He, J. Liu, Y. Chen, M. Ma, L. Zhang, J. Shi, *J. Am. Chem. Soc.* **2012**, *134*, 5722.
[12] Q. Zhang, T. Zhang, J. Ge, Y. Yin, *Nano Lett.* **2008**, *8*, 2867.
[13] Y. Chen, H. R. Chen, L. M. Guo, Q. J. He, F. Chen, J. Zhou, J. W. Feng, J. L. Shi, *ACS Nano* **2010**, *4*, 529.
[14] a) Z. Luo, X. Ding, Y. Hu, S. Wu, Y. Xiang, Y. Zeng, B. Zhang, H. Yan, H. Zhang, L. Zhu, J. Liu, J. Li, K. Cai, Y. Zhao, *ACS Nano* **2013**, *7*, 10271; b) X. Fang, C. Chen, Z. Liu, P. Liu, N. Zheng, *Nanoscale* **2011**, *3*, 1632.
[15] a) Y. J. Wong, L. Zhu, W. S. Teo, Y. W. Tan, Y. Yang, C. Wang, H. Chen, *J. Am. Chem. Soc.* **2011**, *133*, 11422; b) W. Fan, B. Shen, W. Bu, F. Chen, K. Zhao, S. Zhang, L. Zhou, W. Peng, Q. Xiao, H. Xing, J. Liu, D. Ni, Q. He, J. Shi, *J. Am. Chem. Soc.* **2013**, *135*, 6494.
[16] a) K. A. Abel, J. C. Boyer, F. van Veggel, *J. Am. Chem. Soc.* **2009**, *131*, 14644; b) Y. I. Park, J. H. Kim, K. T. Lee, K. S. Jeon, H. Bin Na, J. H. Yu, H. M. Kim, N. Lee, S. H. Choi, S. I. Baik, H. Kim, S. P. Park, B. J. Park, Y. W. Kim, S. H. Lee, S. Y. Yoon, I. C. Song, W. K. Moon, Y. D. Suh, T. Hyeon, *Adv. Mater.* **2009**, *21*, 4467.
[17] S.-K. Ko, X. Chen, J. Yoon, I. Shin, *Chem. Soc. Rev.* **2011**, *40*, 2120.